Chapter 14
Influence of Dynamic Multiaxial Transverse Loading on Dyneema® SK76 Single Fiber Failure

Frank David Thomas, Stephen L. Alexander, C. Allan Gunnarsson, Tusit Weerasooriya, and Subramani Sockalingam

Abstract The primary objective of this research is to investigate, through fundamental experiments, the dynamic multiaxial deformation, failure and strength degradation mechanisms that govern individual ballistic fiber failure. Predicting ballistic impact performance of armor systems requires an understanding of fiber failure under complex multiaxial loading conditions. This study examines the failure behavior of ultrahigh molecular weight polyethylene (UHMWPE) Dyneema® SK76 single fibers under dynamic transverse impact as a function of varying loading rates and projectile geometry. A novel single fiber transverse impact experiment is developed by modifying the Kolsky bar to characterize failure of fibers to create the foundation for a failure model. Experiments are performed with load cells at the fiber ends and with high speed imaging for determining average stresses and strains. Post-test microscopy imaging of failure surfaces are compared to determine the dominant fiber failure modes for each experimental group.

Keywords UHMWPE · Ballistic impact · Transverse compression · High strain rate

14.1 Introduction

Polymeric fibers such as ultra-high molecular weight polyethylene (UHMWPE) are selected for ballistic applications based on their high specific stiffness and specific strength [1, 2]. Characterization of tensile properties of UHMWPE-based material systems have been performed at both quasi-static and high-rate speeds for varying length scales, ranging from single Dyneema® SK76 fibers to full woven fabrics [3, 4]. The knowledge gained through these experiments is incorporated into computer models through the multiscale mechanics of materials approach, which in turn improves predictive modeling capabilities.

For ballistic performance predictions, an understanding of fiber behavior under multiaxial loading is essential. A diverse array of experiments have been performed to quantify various components of the material response of ballistic fiber to multiaxial loading, including quasi-static transverse loading of yarns and individual fibers [5], high strain rate transverse compression and measurement of single filament residual strength at quasi-static and high strain rates [6, 7], and high loading rate transverse impact of yarns [8, 9]. The quasi-static multiaxial loading has been shown to reduce the fiber tensile strength [5–7]. Experimental data combined with representative models have been applied in the development of a strain-based failure criterion for single fiber multiaxial loading at varying strain rates. However, characterizing the transverse loading behavior of individual single fibers at high strain rates is challenging. This chapter details the development of an experimental technique to characterize the failure of single fibers subjected to multiaxial loading as a function of loading rate and geometry.

F. D. Thomas (✉) · S. Sockalingam
McNAIR Center for Aerospace Innovation and Research, University of South Carolina, Columbia, SC, USA

Department of Mechanical Engineering, University of South Carolina, Columbia, SC, USA
e-mail: fthomas@email.sc.edu; SOCKALIN@mailbox.sc.edu

S. L. Alexander
SURVICE Engineering Company, Belcamp, MD, USA
e-mail: stephen.l.alexander18.ctr@mail.mil

C. A. Gunnarsson · T. Weerasooriya
US Army Research Laboratory, Aberdeen Proving Ground, MD, USA
e-mail: carey.a.gunnarsson.civ@mail.mil; tusit.weerasooriya.civ@mail.mil

14.2   Experimental Setup

An experimental technique is developed by modifying the 0.25 inch diameter Kolsky bar to conduct single fiber transverse impact, as shown in Fig. 14.1. The indenter is attached to the incident bar end through a sleeve, and a U frame is used to secure the load cells (Kistler 9712B5) attached to the single fiber mounted on a window frame. A Photron Fastcam SA-5 high speed camera is used to record the deformation. Projectile-fiber contact induces multiaxial loading and strain concentration in the fibers. The setup allows measuring load at failure, strain at failure, failure angle θ, and impact velocity. A series of experiments are performed to characterize fiber failure under dynamic multiaxial loading conditions and to better understand the influence of different projectile geometry (blunt to sharp to razor) on fiber failure.

Diameter measurements are performed on each sample using a confocal optical microscope in a region of the fiber which is proximal to the intended impact location and averaged for use in appropriate stress calculations based on load measurements. As a result, failure at the impact site is a necessary criterion for an experiment to be considered valid in this study.

The fibers are impacted at velocities in the range of 10–20 m/s. Measurements made with camera recordings utilize the overall diameter of the projectile, which is 1 mm, for scale. In order to record at a higher framerate (100,000 fps), resolution is reduced to 320×192. The location of the impactor tip is measured in the initial impact frame and in the frame before failure, and the distance between the two points is divided by the elapsed time to yield the average velocity. A pressure vessel is used to control the velocity, which is filled to specific high and low pressures to vary velocity. Outlier velocities for a given pressure setting are classified as irregular test conditions and are therefore excluded from this study.

Analytical calculations are used to determine strains and strain rates from observed geometric changes. The maximum angle of deflection before failure (θ) provides a useful means of approximating far-field strains (ε) according to Eq. 14.1. Strain rates under the indenter are difficult to evaluate based on the available data, so a hybrid finite element approach must be used to quantify the relationship between strain rate at the failure location and impact velocity. However, for discussion purposes in this chapter, the approximate strain rate (SR) is related to velocity v according to Eq. 14.2, where gage length L_0 is 41.5 mm. The piezoelectric load cells to which the fiber ends are mounted measure axial loads in the fiber at a high frequency and can be used to estimate average stress in the fiber.

$$\varepsilon = \frac{1}{\cos \theta} - 1 \tag{14.1}$$

$$SR = \frac{v}{\frac{1}{2} L_0} \tag{14.2}$$

In order to examine the effects of high-rate multiaxial loading on single UHMWPE fibers, several indenters with varying loading geometries have been designed and manufactured through wire EDM. Loading geometry in all cases is circular and altered by changing the radius in orders of magnitude relative to the fiber diameter. The average fiber diameter of Dyneema® SK76 is measured to be 17.7 μm. The sharp indenter has a radius on the same order of magnitude as the fiber diameter
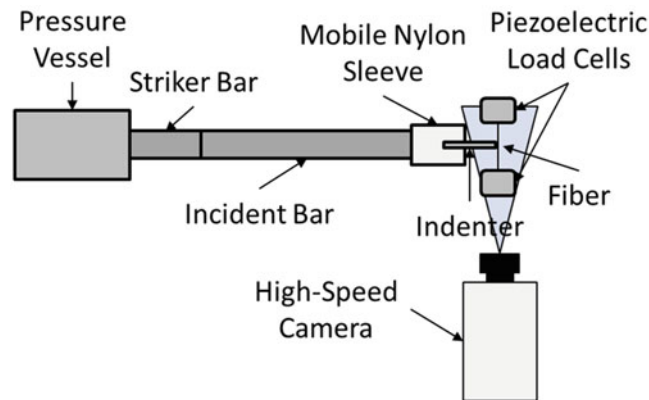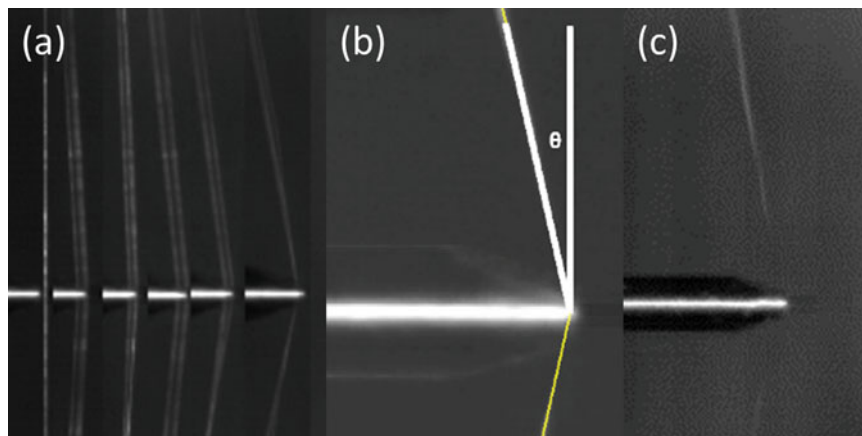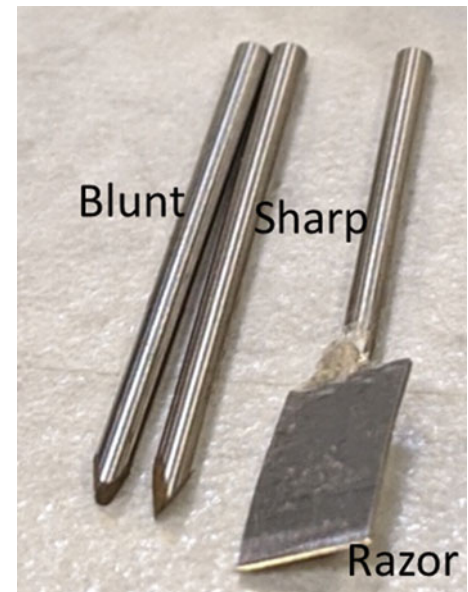

Fig. 14.1 Schematic of experimental setup

Fig. 14.2 Indenter geometry
comparison

Fig. 14.3 Experimental image analysis. (**a**) Progressive loading of single fiber. Images range from undeformed state (far left) to final ultimate tensile strain before failure (far right). (**b**) Angle measurement in final frame before failure. (**c**) Fiber motion post-failure

at approximately 20.0 µm. The blunt indenter is one order of magnitude larger with a radius of 200.0 µm, and the razor indenter is one order smaller at approximately 2.0 µm radius. The indenters as produced are depicted in Fig. 14.2. For each loading geometry, a minimum of 10 successful tests at each loading velocity were performed.

14.3 Results and Discussion

Tests are split into 6 groups based on a combination of impact velocity (fast or slow) and indenter geometry (blunt, sharp, or razor). Each test group contains a minimum of 10 samples in each. Figure 14.3 represents a typical test progression as used for measuring velocity and failure strain. Fast tests correspond to velocities of approximately 20 m/s with a pressure set point of 15 psi, and slow tests correspond to an impacting velocity of approximately 10 m/s with a pressure set point of 5 psi. Average velocities for all groups with standard deviation are displayed in Fig. 14.4.

Sanborn et al. have performed tensile testing of Dyneema® SK76 single fibers at varying gage lengths and strain rates, the results of which are included in Fig. 14.5 [3]. Based on this study, as strain rate increases in uniaxial tension, failure strain decreases, but apparent strength increases, presumably due to rate-dependent stiffness increase. Average experimental strain

Average Velocity with Standard Deviation
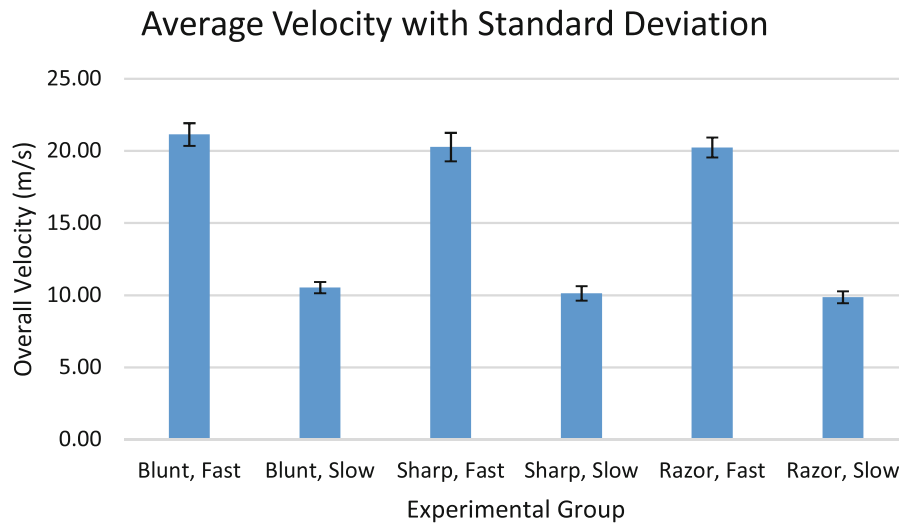
Fig. 14.4 Test velocity comparison

Rate Effects on Maximum Tensile Strain and Strength
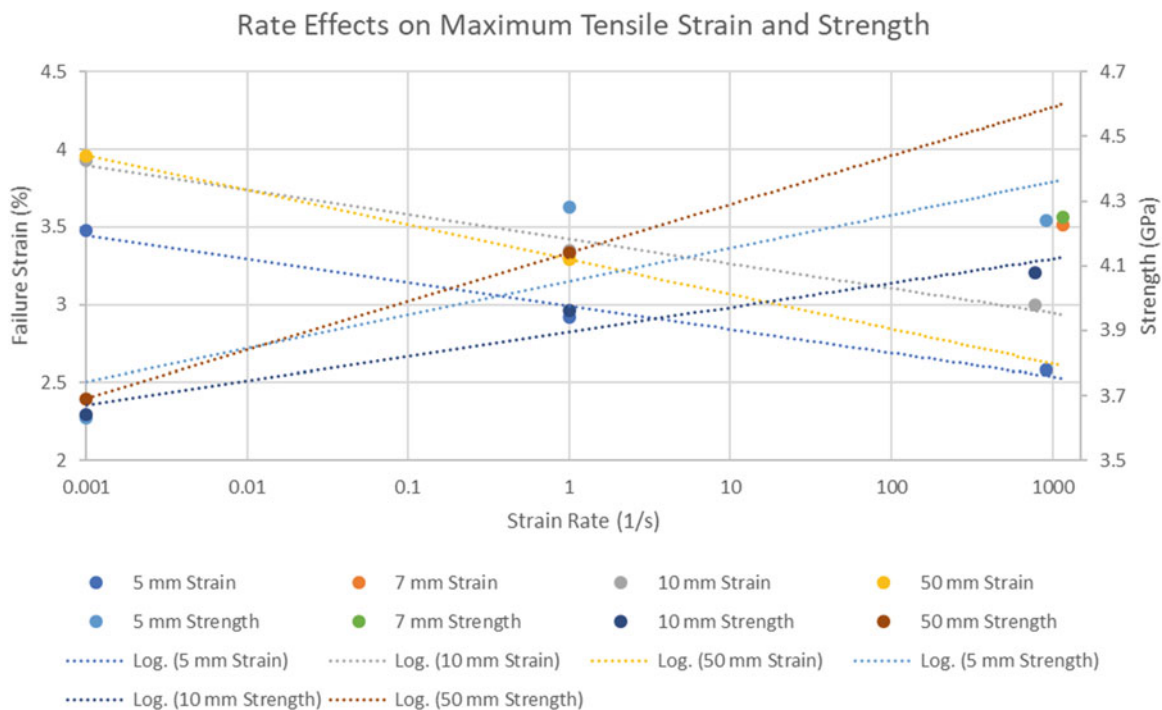
Fig. 14.5 Summary of Sanborn et al. Failure strain decreases with increasing strain rate while apparent strength increases [3]

values calculated using Eq. 14.1 are displayed in Fig. 14.6 with comparison to comparable tensile data. Strength values are calculated based on the average of the maximum loads recorded by each load cell before fiber failure divided by the average diameter at the point of impact. Representative load curves for each group are displayed in Fig. 14.7. Average stress values and standard deviations are displayed in Fig. 14.8 with comparable tensile data. Sample sizes and graph data are summarized in Table 14.1. Controlling for geometry, both strength and failure strain reduce with increase in nominal strain rate.

Broken fiber ends were imaged via light microscopy, and representative images are displayed in Fig. 14.9. Visible damage varies largely according to loading geometry but not so much with average strain rate, with blunt indenters inducing highly visible fibrillation, sharp indenters producing shorter fibrillation (as indicated by the greater magnification on those images), as well as some fibril shearing, and razor indenters producing little to no fibrillation.

Average Strain with Standard Deviation
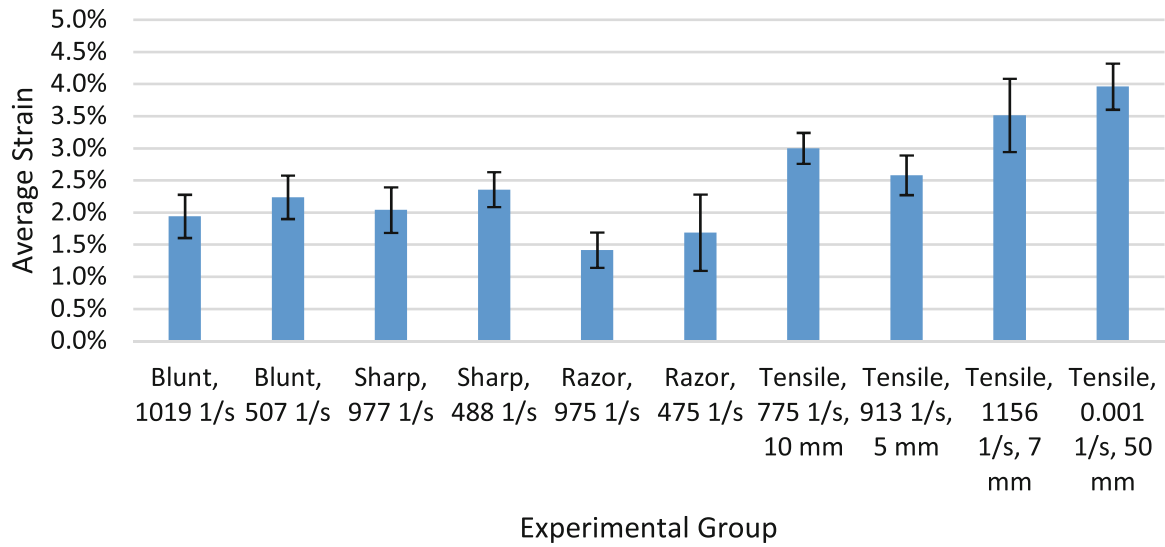

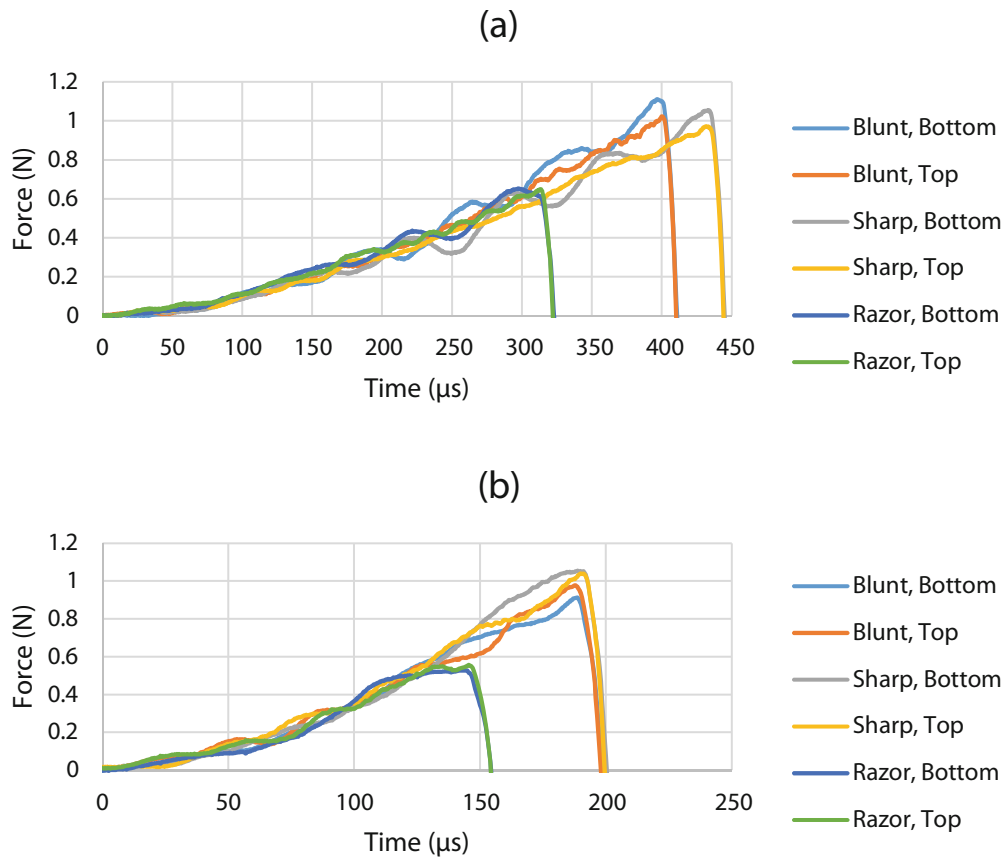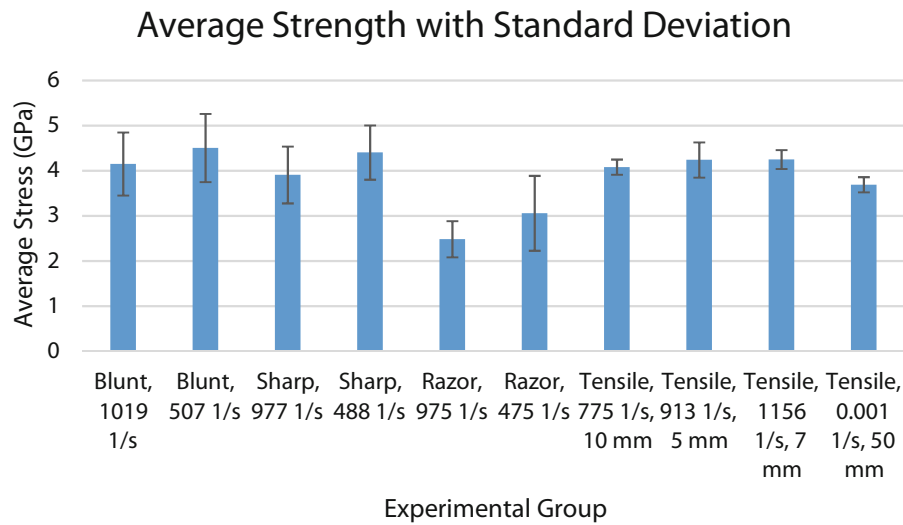**Fig. 14.6** Average strain comparison. Tensile values are from Ref. [3]

(a)

(b)

Fig. 14.7 Representative load cell traces for (**a**) 10 m/s impact velocity (475–507 s^{-1} approximate strain rate) and (**b**) 20 m/s impact velocity (975–1019 s^{-1} approximate strain rate)

Average Strength with Standard Deviation

Fig. 14.8 Average stress comparison. Tensile values are from Ref. [3]

Table 14.1 Experimental data summary. Strain rate is included for correlation with velocity

Transverse impact			Velocity (m/s)		Strain rate (s^{-1})	Strain (%)		Strength (GPa)	
Geometry	Speed	Sample size	Avg	SD	Avg	Avg	SD	Avg	SD
Blunt	Fast	10	21.14	0.79	1018.6	1.94	0.34	4.15	0.70
	Slow	14	10.52	0.40	507.2	2.24	0.34	4.50	0.75
Sharp	Fast	21	20.27	0.99	976.8	2.04	0.36	3.91	0.63
	Slow	15	10.12	0.50	487.9	2.36	0.27	4.40	0.60
Razor	Fast	10	20.24	0.69	975.4	1.42	0.27	2.48	0.40
	Slow	16	9.86	0.41	475.1	1.55	0.57	3.06	0.83
Tensile data			Gage length (mm)		Strain rate (s^{-1})	Strain (%)		Strength (GPa)	
			Avg		Avg	Avg	SD	Avg	SD
			10		775	3.00	0.24	4.08	0.17
			5		913	2.58	0.31	4.54	0.39
			7		1156	3.51	0.57	4.25	0.21
			50		0.001	3.96	0.36	3.69	0.17

14.4 Conclusions

This study examines the effects of loading geometry and loading rate on the failure of UHMWPE Dyneema® SK76 single fibers by developing a modified Kolsky bar experimental technique to transversely impact the single fibers. For all geometries, an increased loading rate resulted in a decrease in both failure strain and apparent strength. For tests at approximately 1000 s^{-1} strain rates, the sharp indenter (20 µm radius) resulted in a 5.07% increase in failure strain and a 5.28% decrease in strength relative to the blunt indenter (200 µm radius) and the razor (2 µm radius) resulted in a 27% decrease in failure strain and a 40% decrease in strength relative to the blunt indenter. For the blunt indenter, failure strain was reduced by 43.5% at 507 s^{-1} and 51.0% at 1019 s^{-1} relative to quasi-static tensile experiments. For the blunt indenter at 507 s^{-1}, failure strain was reduced by 25.5% relative to the 775 s^{-1} tensile experiments at 10 mm gage length, and for the blunt indenter at 1019 s^{-1}, failure strain was reduced by 24.8% relative to the 913 s^{-1} tensile experiments at 5 mm gage length and 44.8% relative to the 1156 s^{-1} tensile experiments at 7 mm gage length. The slight increase in the failure strain for the sharp indenter at both nominal strain rates indicates that the radius is not small enough to induce total shear failure of the fiber like the razor, yet the geometry is influencing the failure mechanism such that the average strain can be increased, possibly at the expense of increased progressive damage through localized failure. For tests at approximately 500 s^{-1}, the sharp indenter demonstrated a 5.36% increase in failure strain and a 2.24% decrease in strength relative to the blunt indenter and the razor demonstrated a 24.53% decrease in failure strain and a 32.09% decrease in strength relative to the blunt indenter. For the blunt indenter, strength was increased by 22.1% at 507 s^{-1} and 12.5% at 1019 s^{-1} relative to quasi-static tensile experiments. For the blunt indenter at 507 s^{-1}, strength was reduced by 10.4% relative to the 775 s^{-1} tensile experiments at 10 mm gage length, and for
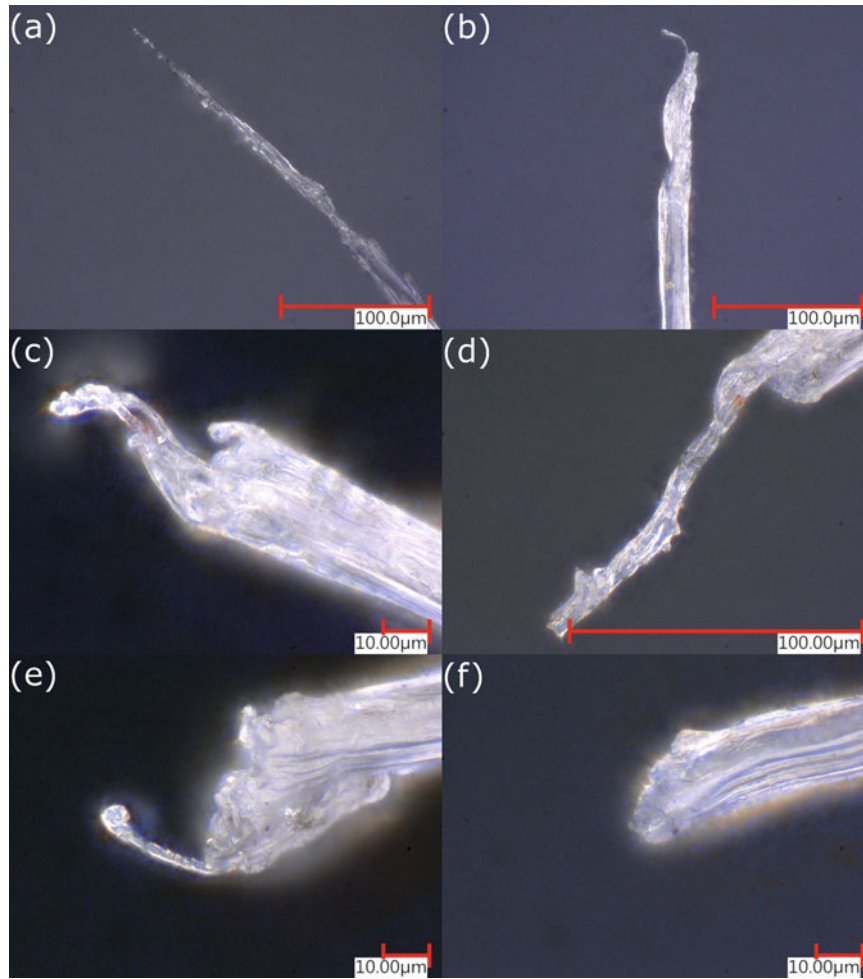
Fig. 14.9 Broken fiber ends for each experimental case: (**a**) blunt, 1018.6 s^{-1}; (**b**) blunt, 507.2 s^{-1}; (**c**) sharp, 976.8 s^{-1}; (**d**) sharp, 487.9 s^{-1}; (**e**) razor, 975.4 s^{-1}; (**f**) razor, 475.1 s^{-1}

the blunt indenter at 1019 s^{-1}, failure strain was reduced by 2.1% relative to the 913 s^{-1} tensile experiments at 5 mm gage length and 2.4% relative to the 1156 s^{-1} tensile experiments at 7 mm gage length. The consistency of the geometric effects when controlling for strain rate indicate the reliability of the results despite relatively large standard deviations. Therefore, the slight decrease in apparent strength in the sharp indenter experiments relative to the blunt indenter for both strain rates despite the increase in apparent strain further supports the conclusion that the indenter geometry is influencing the failure mode even though the differences in the strength and strain data are subtle.

The microscope imaging is useful in elucidating failure modes of the fibers. Blunt tests clearly undergo fibrillation similar to tensile tests. For razor loading, fibrils are much more likely to shear, which appears to occur at significantly smaller levels of deformation. Sharp tests, in contrast to both, demonstrate a combination of fibrillation and fibril shear. This phenomenon could explain the apparent mismatch between failure strain and strength in the case of the sharp experiments compared to the blunt experiments, where failure strain was increased slightly, yet strength was reduced. Initially impacted fibrils may undergo shear failure while fibrils that are not on the impact side fail later due to fibrillation. Strain localization may not be significant enough to result in early macroscopic fiber failure but the reduced load-carrying capacity would result in lower apparent failure stress. Further modeling efforts may yield more information regarding the stress-strain states, strain concentration, and the level of multiaxial loading experienced by the fibers. Future investigation using finite element modeling of the experiments is necessary to develop a strain rate–dependent multiaxial failure criterion [7].

References

1. Krishnan, K., Sockalingam, S., Bansal, S., Rajan, S.D.: Numerical simulation of ceramic composite armor subjected to ballistic impact. Compos. Part B Eng. **41**(8), 583–593 (2010)
2. Sockalingam, S., Chowdhury, S.C., Gillespie, J.W., Keefe, M.: Recent advances in modeling and experiments of Kevlar ballistic fibrils, fibers, yarns and flexible woven textile fabrics – a review. Text. Res. J. **87**(8), 984–1010 (2017)
3. Sanborn, B., DiLeonardi, A.M., Weerasooriya, T.: Tensile properties of Dyneema SK76 single fibers at multiple loading rates using a direct gripping method. J. Dyn. Behav. Mater. **1**(1), 4–14 (2015)
4. Wang, H., et al.: Tensile properties of ultra-high-molecular-weight polyethylene single yarns at different strain rates. J. Compos. Mater. (2019)
5. Hudspeth, M., Li, D., Spatola, J., Chen, W., Zheng, J.: The effects of off-axis transverse deflection loading on the failure strain of various high-performance fibers. Text. Res. J. **86**(9), 897–910 (2015)
6. Sockalingam, S., Thomas, F.D., Casem, D., Gillespie, J.W., Weerasooriya, T.: Failure of Dyneema® SK76 single fiber under multiaxial transverse loading. Text. Res. J. (2018)
7. Thomas, F.D., Casem, D., Weerasooriya, T., Sockalingam, S., Gillespie Jr., J.W.: Influence of high strain rate transverse compression on the tensile strength of polyethylene ballistic single fibers. **1**, 339–344 (2019)
8. Smith, J.C., Fenstermaker, C.A., Shouse, P.J.: Stress-strain relationships in yarns subjected to rapid impact loading. Text. Res. J., 743–757 (1965)
9. Roylance, D.: Ballistics of transversely impacted fibers. Text. Res. J. **47**(10), 679–684 (1977)